Available online at www.sciencedirect.com
ScienceDirect
Journal of Nuclear Materials 366 (2007) 178–186
journal of nuclear materials
www.elsevier.com/locate/jnucmat

Modelling isothermal and non-isothermal recrystallisation kinetics: Application to Zircaloy-4

J.W.C. Dunlop [a,*], Y.J.M. Bréchet [b], L. Legras [c], H.S. Zurob [d]

[a] Department of Biomaterials, Max Planck Institute of Colloids and Interfaces, 14424 Potsdam, Germany
[b] Laboratoire de Thermodynamique et Physico-Chimie Métallurgiques, Domaine Universitaire, BP 75, 38402 St. Martin d'Hères cedex, France
[c] Electricité de France, R&D Division, Material and Mechanics of Components Department, Les Renardières, 77818 Moret sur Loing cedex, France
[d] Department of Materials Science and Engineering, McMaster University, 1280 Main Street West, Hamilton, ON, Canada L8S 4L7

Received 10 October 2006; accepted 15 December 2006

Abstract

This paper considers the modelling of recovery and recrystallisation of single phased metals. The recrystallisation nucleation model of Zurob et al. [H. Zurob, Y. Bréchet, J. Dunlop, Acta Mater. 54 (2006) 3983] has been extended to allow for recrystallisation growth and the concurrent recovery in the non-recrystallised grains. The input parameters of the model are physically based and can be measured, being the recovery kinetics and boundary mobility. Output from the model gives critical strains and temperatures for recrystallisation, and the recrystallisation kinetics. As an example the model is applied to the recovery and recrystallisation kinetics of Zircaloy-4. The grain boundary mobility is not well known for this material, and so it is taken to be a free parameter with a temperature dependence coming from the Turnbull mobility. The model successfully describes recovery kinetics of Zircaloy-4, and once the mobility has been estimated gives good predictions of critical temperatures and strains as well as the kinetics of recrystallisation under non-isothermal heat treatments.

1. Introduction

The modelling of the softening kinetics of work hardened materials has important industrial applications both for fabrication and for the prediction of in service performance. The standard tool to model phenomenologically the evolution of the recrystallised fraction, $X(t)$, during annealing is the Johnson–Mehl–Avrami–Kolmogorov (JMAK) equation [1–5]

$$X(t) = 1 - \exp(-kt^n), \tag{1}$$

where t is the time and, k and n are numerical constants used to fit the equation to the experimental data. The JMAK equation efficiently describes softening data and recrystallisation kinetics for isothermal heat treatments, however it is difficult to assign an unambiguous physically significant meaning to

* Corresponding author.
E-mail address: john.dunlop@mpikg.mpg.de (J.W.C. Dunlop).

0022-3115/$ - see front matter © 2007 Elsevier B.V. All rights reserved.
doi:10.1016/j.jnucmat.2006.12.074

the parameters k and n. The standard interpretations relies on simplistic and probably unrealistic assumptions such as site saturation, or constant nucleation rate and constant growth kinetics. Experimentally, and not surprisingly, the measured n exponent is far from the values expected using these assumptions (i.e. 3–4) [6]. It is however well known that the nucleation rate is non-constant [6–9] and that recovery takes place concurrently with recrystallisation leading to a non-constant driving force and therefore to a non-constant growth rate. In the present paper a general approach is proposed to relax these constraints, by coupling the driving force for recrystallisation with a model for static recovery and using a more explicit description of the process of recrystallisation nucleation. This requires a more sophisticated mathematical treatment (Schneider equations [10]) but provides a model which can be readily extended to non-isothermal conditions. This approach is then applied to the recrystallisation kinetics of the zirconium alloy Zircaloy-4.

Section 2 describes the development of a general mean field model for recovery kinetics in conjunction with nucleation and growth of recrystallisation. The nucleation of new grains is related to a microstructural instability of the underlying cell/sub-grain structure. In the growth model, the driving force for recrystallisation is taken to be the stored energy due to cold work which decreases due to static recovery. Therefore the growth rate of new grains decreases with time due to the changing driving force. The model is then applied (Section 3) to predict the nucleation of recrystallisation and the isothermal softening kinetics of Zircaloy-4 using physically significant parameters for which the order of magnitude is known. The model is then applied to non-isothermal recrystallisation kinetics of Zircaloy-4.

2. A general model for recrystallisation kinetics

2.1. Nucleation of recrystallisation

The nucleation of recrystallisation is described using the model of Zurob et al. [11] which enables the prediction of nucleation rates and incubation times for recrystallisation from a knowledge of recovery kinetics, initial sub-grain sizes and dislocation density and sub-grain boundary mobility. In this approach nucleation of recrystallisation is taken to occur due to strain induced boundary migration (SIBM). The main features of the model are now recalled, the reader is referred to [11] for detailed explanations, for other nucleation processes see [6]. The sub-grain structure of the deformed state can be described by the average size, $\langle r\rangle$, and the cell size distribution $P(r)$. A given cell or sub-grain of size $r(t)$ will start to grow in an unstable manner within the deformed structure, when the driving force for growth, $G(t)$, overcomes the capillary forces $2\gamma_{SE}/r(t)$, where γ_{SE} is the surface energy. This is the Bailey–Hirsch criterion [12], which gives a critical sub-grain/cell size $r_c(t)$ above which unstable growth, and thus nucleation, occurs

$$r_c(t) > \frac{2\gamma_{SE}}{G(t)}. \tag{2}$$

Only the sub-grains larger than this critical size, will be able to provide viable nuclei within a time t. During annealing, the average sub-grain size, $\langle r(t)\rangle$, increases with time, t, as [6,13]

$$\langle r(t)\rangle = \langle r_0\rangle + \int_0^t M_{sg}G(t)\mathrm{d}t, \tag{3}$$

where $\langle r_0\rangle$ is the initial average sub-grain size, and M_{sg}, is the average mobility of the sub-grain boundary, which is of the order of 0.01–1 of the high angle boundary mobility, M_{HAGB} [11]. $G(t)$ is the stored energy which decreases with time due to static recovery.

The fraction of sub-grains and cells that can form viable nuclei can be obtained by integration from $r_c(t)$ to infinity of the size distribution, $P(r)$

$$f(t) = \int_{r_c(t)}^{\infty} P(r)\mathrm{d}r. \tag{4}$$

Hansen and co-workers [14,15] measured sub-grain distributions for a variety of materials in different deformation states and shows that sub-grain distributions observe self-similar scaling laws. A self-similar size distribution of sub-grains during growth amounts to expressing $P(r)$ as

$$P(r) = \widetilde{P}(\chi)\frac{\mathrm{d}\chi}{\mathrm{d}r} = \widetilde{P}(\chi)\frac{1}{\langle r\rangle}, \tag{5}$$

where χ is the sub-grain/cell size normalised by the average sub-grain/cell size $\langle r\rangle$. The normalised size distribution can be described by a Rayleigh distribution [16]

$$P(\chi) = \frac{\pi}{2}\chi\exp\left(-\frac{\pi\chi^2}{4}\right). \tag{6}$$

The Maxwell distribution could also be used but the Rayleigh distribution provides a better fit to the

experimental data [16]. The fraction, $f(t)$, of sub-grains that have reached the critical size for nucleation at time t, is therefore

$$f(t) = \int_{\chi_c(t)}^{\infty} P(\chi)\mathrm{d}\chi, \tag{7}$$

where $\chi_c(t)$ is the normalised critical sub-grain size. The fraction of sub-grains that can act as recrystallisation nuclei is finally

$$f(t) = \exp\left(-\frac{\pi}{4}\chi_c(t)^2\right). \tag{8}$$

The number of nuclei per unit volume is calculated by assuming that all nuclei will form on grain boundaries of the deformed material, and the number of possible sites for nucleation per unit surface scales as $1/\langle r(t)^2\rangle$. An approximate estimate for the number of sub-grains $N_{sg}(t)$, touching the grain boundary per unit volume, is the deformed grain boundary area per unit volume $S(t)$, divided by the average area of the sub-grain/cell

$$N_{sg}(t) = \frac{S(t)}{\pi\langle r(t)^2\rangle}. \tag{9}$$

The deformed grain boundary area per unit volume as a function of initial grain size D_i, and cold rolling strain, ε is described using the empirical formulae of Senuma et al. [17]

$$S_0(D_i,\varepsilon) = \frac{24}{\pi D_i}(0.491\mathrm{e}^{\varepsilon} + 0.155\mathrm{e}^{-\varepsilon} + 0.143\mathrm{e}^{-3\varepsilon}). \tag{10}$$

This formula describes the change in shape of a spherical grain to an ellipsoid during rolling deformation. From this the evolution of the number of nuclei per unit volume $N(t)$, as a function of time can be readily calculated

$$N(t) = f(t)N_{sg}(t) \tag{11}$$

and thus the nucleation rate per unit volume $\dot{N}(t)$.

In order to go further it is necessary to evaluate the evolution of the stored energy $G(t)$, resulting from static recovery.

2.2. Recovery kinetics

Static recovery is classically described as the relaxation processes of the internal stresses, associated with the dislocation population resulting from cold work. The initial model proposed by Kuhlmann et al. [18] and Friedel [19] directly leads to a logarithmic decrease of the flow stress. This model was modified in order to account explicitly for the evolution of dislocation density by Verdier et al. [20]

$$\frac{\mathrm{d}\tilde{\sigma}}{\mathrm{d}t} = -E\frac{\tilde{\sigma}^2}{M_{\mathrm{Taylor}}^3\alpha^2\mu^2}v_D \times \exp\left(-\frac{U_0}{k_B T}\right)\sinh\left(\frac{\tilde{\sigma}v}{k_B T}\right), \tag{12}$$

where E is Young's modulus, M_{Taylor} is the Taylor factor, α is 0.3, μ is the shear modulus, v_D is the Debye frequency, k_B is the Boltzmann constant, T is the absolute temperature, U_0 is the activation energy and v is the activation volume. $\tilde{\sigma}$, is the dislocation forest contribution to the flow stress and is related to the dislocation density, ρ_f, by

$$\tilde{\sigma} = M_{\mathrm{Taylor}}\alpha\mu b\sqrt{\rho_f}, \tag{13}$$

where b is the Burger's vector. From the evolution of $\tilde{\sigma}$, the evolution of dislocation density is immediately derived and the stored energy of cold work, is calculated as

$$G(t) = \frac{1}{2}\rho_f(t)\mu b^2. \tag{14}$$

The full form of this equation depends on the nature of the dislocation and includes a logarithmic term containing inner and outer cut-off radii, within which the line energy is calculated. Humphreys and Hatherly [6] argue that for typical values of cut-off radii and for average dislocation populations, the logarithmic term can be neglected giving rise to a factor of a half, an approximation which is used in the following calculations.

2.3. Growth kinetics

Once a sub-grain has reached the critical size for nucleation (Eq. (3)), it will grow into the deformed matrix if it has access to a boundary of sufficient mobility. The growth rate of a given grain is taken to be

$$v(t) = M_{gb}G(t), \tag{15}$$

where M_{gb} is the average grain boundary mobility. The size (radius) $r(t)$, of a given grain at time t, nucleated at time t', will then be the initial radius of the grain at nucleation $r_0(t)$, plus the increase in radius due to growth at rate $V(t)$, between times t and t'

$$r(t',t) = r_0(t') + \int_{t'}^{t} M_{gb}G(t'')\mathrm{d}t''. \tag{16}$$

The initial grain radius at nucleation is given by the critical radius for nucleation, Eq. (3), which gives with Eq. (16) the grain radius at time t' as

$$r(t',t) = \frac{2\gamma_{SE}}{G(t')} + \int_{t'}^{t} M_{gb} G(t'')\mathrm{d}t''. \quad (17)$$

Assuming that the grains are spherical and that their growth rate is isotropic, then the volume of a grain at time t, nucleated at time t' is

$$V(t',t) = \frac{4\pi}{3}\left(\frac{2\gamma_{SE}}{G(t')} + \int_{t'}^{t} M_{gb} G(t'')\mathrm{d}t''\right)^3. \quad (18)$$

The assumption of spherical crystallites is supported by the equiaxed microstructure observed after complete recrystallisation. If necessary, the effect of grain geometry can be considered by introducing a corrective factor (for simple geometries see [21]).

2.4. Global recrystallisation kinetics, isothermal case

From the nucleation rate and the growth rate one still has to deal with the impingement problem, before obtaining the global recrystallisation kinetics. The volume, $\phi(t,t')$, of grains at time t, nucleated at time t', is simply the number of nuclei formed at time t', multiplied by the volume of each grain

$$\phi(t,t')\mathrm{d}t' = (\dot{N}(t')\mathrm{d}t')\frac{4\pi}{3}\left(\frac{2\gamma_{SE}}{G(t')} + \int_{t'}^{t} M_{gb} G(t'')\mathrm{d}t''\right)^3. \quad (19)$$

The extended volume fraction, $\phi(t)$ is obtained by integrating between time 0 and t

$$\phi(t) = \frac{4\pi}{3}\int_0^t \dot{N}(t')\left(\frac{2\gamma_{SE}}{G(t')} + \int_{t'}^{t} M_{gb} G(t'')\mathrm{d}t''\right)^3 \mathrm{d}t'. \quad (20)$$

The actual recrystallised volume fraction $X(t)$, is given by

$$X(t) = 1 - \exp(-\phi(t)). \quad (21)$$

The usual derivation of JMAK equation is straightforward from the previous equations under the simplifying assumptions of a constant nucleation rate or constant number of nucleation sites (site saturation) and a constant growth rate. In the most general case, the situation that has to be dealt with is considerably more difficult, and requires solving a double integral equation. A mathematical technique allowing a numerically efficient solution of the problem was found by Schneider in the context of polymer crystallisation [10]. The details of the procedure is to be found in Refs. [22–25].

Schneider et al. [10], by applying the ideas of Tobin [26,27], developed a method to solve the equivalent of Eq. (20). By repetitive differentiation of Eq. (20) the double integral can be converted into a series of coupled differential equations, which in turn are easily solvable numerically. The advantage is that these equations can be integrated solely with respect to time, and the problem of the double integration over time and nucleation time is removed.

The extended volume fraction is rewritten in the form of the following Minkowski functional:

$$\Psi_\mu(t) = \frac{8\pi}{(3-\mu)!}\int_0^t \dot{N}(t') \times \left(\frac{2\gamma_{SE}}{G(t')} + \int_{t'}^{t} M_{gb} G(t'')\mathrm{d}t''\right)^{3-\mu} \mathrm{d}t'. \quad (22)$$

The geometrical interpretation of each order of Minkowski functional is given in Table 1. The rate equation for $\Psi_\mu(t)$ can be expressed as a function of $\Psi_{\mu+1}(t)$. The extended volume fraction $\phi(t)$ is exactly identical to the zeroth order Minkowski functional and can be obtained after three successive integrations of the Ψ-function of higher order.

2.5. Global recrystallisation kinetics, non-isothermal case

The incorporation of non-isothermal conditions into the rate equations is straightforward provided the temperature dependence of the elementary step is known [10]. The temperature dependence of recrystallisation nucleation arises from the tempera-

Table 1
The four rate equations describing the evolution of the Minkowski functionals for recrystallisation and their geometrical significance

Functional order (μ)	Rate equation	Geometric significance
0	$\dot{\Psi}_0(t) = \pi\frac{32\gamma_{SE}^3\dot{N}(t)}{3G(t)^3} + M_{gb}G(t)\Psi_1(t)$	Extended volume fraction
1	$\dot{\Psi}_1(t) = \pi\frac{16\gamma_{SE}^2\dot{N}(t)}{G(t)^2} + M_{gb}G(t)\Psi_2(t)$	Extended surface fraction
2	$\dot{\Psi}_2(t) = \pi\frac{16\gamma_{SE}\dot{N}(t)}{G(t)} + M_{gb}G(t)\Psi_3(t)$	Mean curvature
3	$\dot{\Psi}_3(t) = 8\pi\dot{N}(t)$	Gaussian curvature

ture dependence of static recovery, which is thermally activated, (Eq. (12)), and through the temperature dependence of the boundary mobility's. Mobility plays a role in the growth terms, for subgrain growth (Eq. (2)) and grain growth (Eq. (15)) once nucleation has occurred. It is then sufficient to use a function, $T(t)$, describing the evolution of temperature with time, to update the recovery rate, Eq. (12), and the temperature dependent parameters in the nucleation and growth model at each time step. The temperature dependent parameters are the two elastic modulii, $E(T)$ and $\mu(T)$ (weak dependence), and the boundary mobilities $M_{sg}(T)$, and $M_{gb}(T)$ (strong dependence). The temperature dependence of the elastic modulii is well known for most materials. The mobility is less well characterised, however the Turnbull estimation for mobility [28] can be used as a first approximation to account for the temperature dependence.

3. Application to Zircaloy-4

In this section the model describing the static recovery, recrystallisation nucleation and the kinetics of growth, is applied to the annealing kinetics of cold-worked Zircaloy-4.

Zirconium alloys are used in the nuclear industry due to their low thermal neutron capture cross section and limited corrosion rate [29,30]. In pressurised water reactors, the alloy Zircaloy-4 is commonly used as the cladding material for fuel assemblies. Due to the processing of the Zircaloy-4 fuel tubes (cold pilgering) the alloy is initially cold worked and during service the dislocation hardening increases due to the production of numerous irradiation defects, principally dislocation loops. Although the microstructure is stable during the fuel assemblies life within the reactor (no significant recovery of initial dislocation density at operating temperatures of ~350 °C), post-service conditions may result in cladding temperatures rising well above 400 °C [31,32]. These temperatures can lead to significant softening of Zircaloy-4 due to recovery and recrystallisation, which in turn can have important consequences on the long term behaviour of zirconium cladding during further storage of spent fuel [33]. It is thus important to develop a physically based model for recrystallisation and recovery of Zircaloy-4 which can take into account the non-isothermal conditions expected during post-service.

Zircaloy-4 tubes (diameter ~9.5 mm and wall thickness ~0.6 mm) in the cold worked stress relieved state (cold work of 78%) were tested. The composition of the base alloy Zircaloy-4 is as follows: 1.25 wt% Sn, 0.2 wt% Fe, 0.12 wt% Cr, 1300 ppm O, and 136 ppm C. Isothermal heat treatments were carried out on the tubes under vacuum in the temperature range of 400–520 °C. The results of the model are of course sensitive to the parameter values, however these values have severe restrictions and must lie within the range of physically reasonable values which are known. Some parameters are fixed, as they have been measured experimentally and reported in the literature. Others such as the activation energy and volume for recovery and the temperature dependence of mobility are not so well known, have conflicting values in the literature or cannot be directly measured. The recovery model and the mobility are fitted to experimental data at several temperatures and then checked at other temperatures to ensure consistency. No other parameters were changed or required to describe the critical strains and temperatures or the non-isothermal recrystallisation kinetics, of Hunt and Schulson [34], thus serving as a test of the model and validating the parameters used.

3.1. Recovery kinetics

Although cold-worked Zircaloy-4 softens at temperatures around 400 °C, below approximately 420 °C, no recrystallisation is observed [35]. The softening can thus be directly attributed to static recovery. The kinetics of static recovery are given by Eq. (12). There are two fitting parameters, the activation energy and the activation volume, for which the order of magnitude is known. For Zircaloy-4, the activation energy is taken to be the same as that for self-diffusion 319 kJ/mol. To fit the data an activation volume of $28b^3$ is used which is within the range of physically acceptable values of about $20–50b^3$ [36]. An example of the recovery kinetics at 400 °C is given in Fig. 1 which illustrates the softening kinetics of cold worked Zircaloy-4 compared to the output of the recovery model. The value of U_0 and v allow the accurate description of softening kinetics for all temperatures below 420 °C.

3.2. Global recrystallisation kinetics isothermal case

The model for recrystallisation nucleation and growth described in part 2 is now applied to the isothermal recrystallisation kinetics of Zircaloy-4. The parameters used are detailed in Table 2. In pure

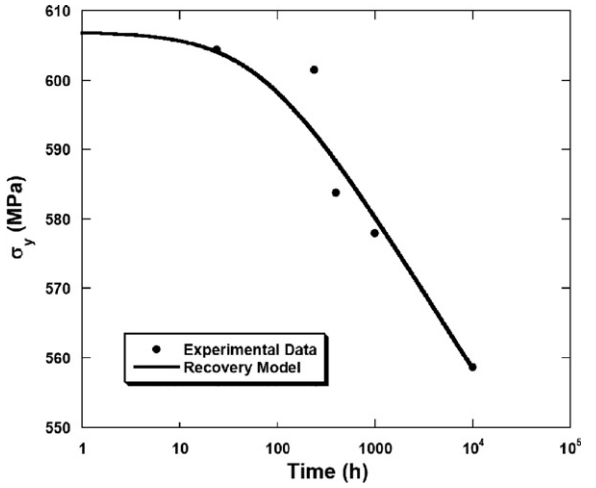

Fig. 1. Comparison of softening kinetics of Zircaloy-4 at 400 °C to the recovery model.

Table 2
Notations and values of parameters for Zircaloy-4

Parameter	Name	Value	References
E	Young's modulus	119.6–0.076 (T) GPa	[53]
μ	Shear modulus	40.86–0.02 (T) GPa	[54]
ν_D	Debye Frequency	5.2×10^{12} Hz	[55]
γ_{SE}	Surface energy	0.22 J m^{-2} (no data for Zircaloy-4)	[6]
D_i	Initial grain size	5×10^{-6} m	
b	Burger's vector	3.23×10^{-10} m	[56]
U_0	Activation energy of recovery	319 kJ/mol	
v	Activation volume for Recovery	$28b^{-3}$	

zirconium Dewobroto et al. [37], using EBSD, showed SIBM on grain boundaries to be a mechanism for nucleation and the assumption that this mechanism holds for Zircaloy-4 will be used in the following. The recovery kinetics from Section 3.1 are used without any changes. An initial grain size of 5 μm was measured using optical microscopy. The measured stress strain curve of Zircaloy-4 was approximated by a power law to give the increase in flow stress as a function of cold-work strain:

$$(\sigma-\sigma_0)=\tilde{\sigma}\cong 238\varepsilon^{0.5}\ \text{MPa}. \tag{23}$$

The initial average sub-grain size $\langle r_0\rangle$ as a function of the amount of work hardening, $(\sigma-\sigma_0)$, is taken from Abson and Jonas [38]

$$\langle r_0\rangle=\frac{8.6\times10^{-5}}{(\sigma-\sigma_0)}. \tag{24}$$

The order of magnitude of the surface energy, γ_{SE}, is known to be between 0.1 and 1 J m^{-2} [6], in the following a fixed value of 0.22 J m^{-2} is used. The remaining parameters required to describe the kinetics of recrystallisation are the average sub-grain boundary and grain boundary mobilities, M_{sg} and M_{gb} respectively. The average sub-grain boundary mobility is given by

$$M_{sg}=\int_0^{\theta_{HAG}}\Phi(\theta)M(\theta)\mathrm{d}\theta, \tag{25}$$

where $\Phi(\theta)$ is the distribution of sub-boundary misorientations, θ_{HAG} is the misorientation at which a sub-grain boundary has the same mobility as a high angle boundary (15°). $M(\theta)$ is the function describing the dependence of mobility on boundary misorientation. Following [11], the average quantity lies between 0.02 and 0.2 of the high angle mobility. As the boundary mobility is not characterised in Zircaloy-4; the model is simplified by assuming that a single mobility M_{ave} can be used for both types of boundaries, M_{ave} being used as an adjustable parameter to fit the model to the experimental data.

Figs. 2 and 3 show the softening kinetics and the recrystallised volume fraction for Zircaloy-4 annealed at different temperatures compared to the output of the model. The experimental data for hardness and the metallographic results are well described by the model.

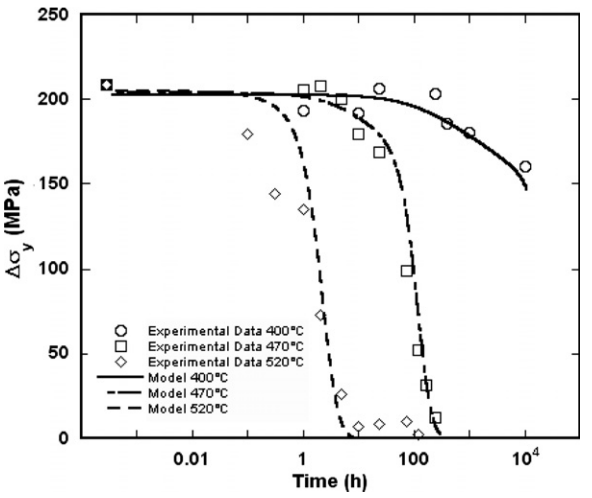

Fig. 2. Softening kinetics of Zircaloy-4 as measured from Vickers hardness compared to the model output.

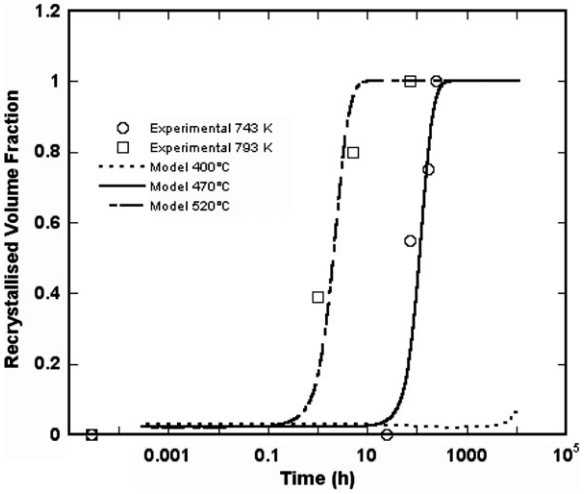

Fig. 3. Recrystallisation kinetics of Zircaloy-4 as measured using optical microscopy compared to the model output.

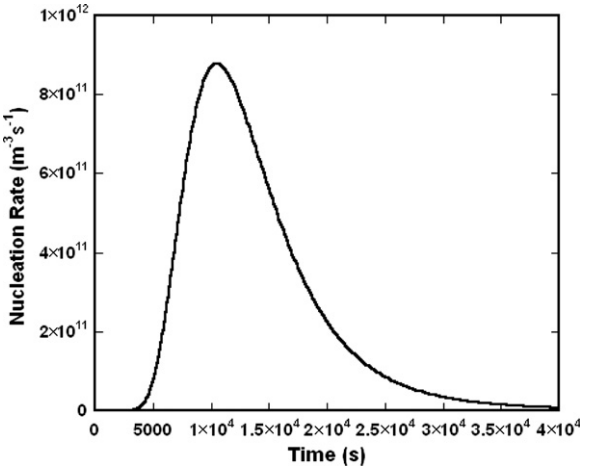

Fig. 4. Nucleation rate as a function of time.

The mobilities used to fit the model to the experimental data are somewhat smaller than those expected from the Turnbull estimate [28]

$$M_{\text{Turnbull}} = \frac{\delta D_{\text{gb}} V_{\text{M}}}{b^2 R_{\text{g}} T}, \tag{26}$$

where δ is the grain boundary thickness ($\sim$1 nm), D_{gb} is the grain boundary diffusion coefficient, R_{g} is the ideal gas constant and V_{M} is the molar volume of Zircaloy-4. This might be due to the solute-drag [39] effect of Sn which is known to slow down the kinetics of recrystallisation in zirconium [29,40–43]. The slow branch of the solute drag model of Cahn [39] can be coupled to the Turnbull mobility giving a mobility M_{Total} of

$$M_{\text{Total}} = \left(\frac{1}{M_{\text{Turnbull}}} + \alpha C_{\text{Sn}}\right)^{-1}, \tag{27}$$

where C_{Sn} is the concentration of tin and

$$\alpha = \frac{\delta N_{\text{v}} (k_{\text{B}} T)^2}{E_{\text{b}} D} \left(\sinh\left(\frac{E_{\text{b}}}{k_{\text{B}} T}\right) - \frac{E_{\text{b}}}{k_{\text{B}} T}\right), \tag{28}$$

where D is the diffusion coefficient of tin, and E_{b} is the binding energy of tin to the grain boundary interface.

In the following two sections the model is applied to the prediction of critical strains and non-isothermal recrystallisation kinetics, without modification of the adjustable parameters.

3.3. Nucleation kinetics, prediction of the critical strains

For a given amount of cold work, the nucleation rate per unit volume can be calculated. This is illustrated in Fig. 4, which shows the nucleation rate for Zircaloy-4 as calculated from the nucleation model as a function of time for different temperatures. The nucleation rate increases with increasing temperature. Similar curves for the nucleation rate have been measured in the literature see e.g. [8,9] for other materials.

A direct output of the nucleation model is the prediction of the recrystallisation temperatures as a function of cold work strain. The recrystallisation temperature, is the temperature above which recrystallisation is observed for a given strain and annealing time, and is often quoted in the literature as a way of characterising the ability of a given material to recrystallise. Fig. 5 illustrates recrystallisation temperatures taken from the literature [44–52] as a function of strain for annealing times of one hour, for alloys of the same type as Zircaloy-4 (i.e. single phase zirconium alloys with approximately 1%Sn in solid solution). Although there is some scatter in the data due to the different experimental techniques, alloys and heat treatment times, a clear trend in recrystallisation temperatures as a function of strain can be seen. The solid line gives the prediction of the recrystallisation temperature for different initial. The output of the model, run with the same values of activation energy, activation volume and boundary mobility as Section 3.2, compares very favourably with the literature results.

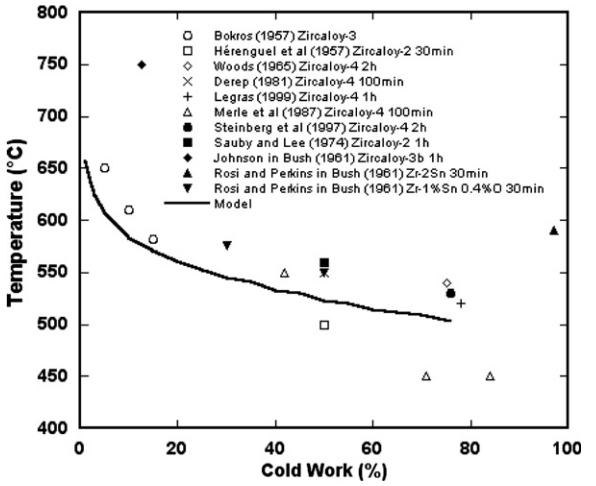

Fig. 5. Critical strain for recrystallisation as a function of temperature.

3.4. Global recrystallisation kinetics non-isothermal case

The model is then applied to the kinetics of recrystallisation under non-isothermal conditions, temperature ramps off 0.5 and 25 K s^{-1}, without introducing any new parameters. The temperature dependence of the mobility is described using the Turnbull mobility coupled to Cahn's model for solute drag (see Section 3.2). It is assumed that the surface energy, γ_{SE}, is constant in the temperature range of interest. The model is tested for the recrystallisation kinetics under two different conditions of constantly increasing temperature (0.5 and 25 K s^{-1}) and compared to the experimental results of Hunt and Schulson [34]. There is a good agreement between the prediction of the model and the experimental data of [34] (see Fig. 6). This indicates that the model has captured the essential ingredients required to describe the recrystallisation kinetics of Zircaloy-4 in a physically realistic and predictive manner.

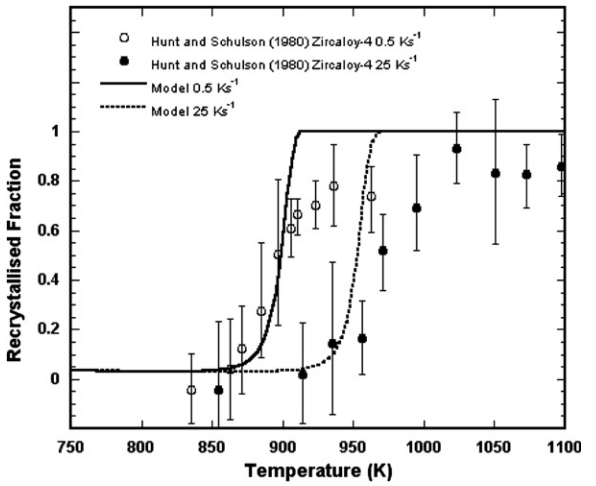

Fig. 6. Comparison of the predicted recrystallised fraction with non-isothermal heat treatments (0.5 K s^{-1} and 25 K s^{-1}) for Zircaloy-4 with the data of Hunt and Schulson [34].

4. Conclusion

We have shown in this paper, a general method to model recrystallisation kinetics in both isothermal and non-isothermal conditions. The physical ingredients of this approach are: a nucleation criterion based on a quantitative analysis of the Bailey–Hirsch mechanisms, a model for static recovery kinetics and a model for the overall kinetics allowing for different degrees of deformation during cold-rolling, non-constant nucleation rates, and non-constant growth rates.

This model was applied successfully to the case of Zircaloy-4 allowing predictions for critical strains as a function of annealing temperature, and for recrystallisation kinetics both isothermal and non-isothermal.

This model is general enough to be applied to other single phase materials (copper, aluminium solid solutions), providing that strain induced boundary migration remains the main nucleation mechanism. It could also be extended in order to predict not only the recrystallised volume fraction but also grain sizes.

Acknowledgement

Electricité de France is gratefully acknowledged for the financial support of J.D.

References

[1] M. Avrami, J. Chem. Phys. 7 (1939) 1103.
[2] M. Avrami, J. Chem. Phys. 8 (1940) 212.
[3] M. Avrami, J. Chem. Phys. 9 (1941) 177.
[4] W.A. Johnson, R.F. Mehl, Trans. AIMME 135 (1939) 416.
[5] A.N. Kolmogorov, Isv. Akad. Nauk SSSR. Ser. Math. 1 (1937) 355.
[6] F. Humphreys, M. Hatherly, Recrystallization and Related Annealing Phenomena, Pergamon, Oxford, 1995.
[7] W.A. Anderson, R.F. Mehl, Trans. Am. Inst. Mining Met. Eng., Inst. Metals Div., Tech. Pub. 161 (1945) 140.
[8] E. Lauridsen, H. Poulsen, S. Nielsen, D. Juul Jensen, Acta Mater. 51 (2003) 4423.

[9] F. Humphreys, Nucleation in recrystallisation, in: B. Bacroix, J. Driver, R. Le Gall, C. Maurice, R. Penelle, H. Réglé (Eds.), Recrystallisation and Grain Growth, vol. 1, Trans Tech., Annecy, 2004, p. 629.
[10] W. Schneider, A. Köppl, J. Berger, Int. Polym. Proc. 2 (1988) 151.
[11] H. Zurob, Y. Bréchet, J. Dunlop, Acta Mater. 54 (2006) 3983.
[12] J.E. Bailey, P.B. Hirsch, Proc. R. Soc. Lond. A 267 (1962) 11.
[13] R. Sandström, Acta Metall. 25 (1977) 897.
[14] D. Hughes, N. Hansen, Phil. Mag. 83 (2003) 3871.
[15] D. Hughes, D.C. Chrzan, C. Liu, N. Hansen, Phys. Rev. Lett. 81 (21) (1998) 4664.
[16] W. Pantleon, N. Hansen, Acta Mater. 49 (8) (2001) 1479.
[17] T. Senuma, H. Yada, Y. Matsumura, T. Futamura, Tetsu to Hagane 70 (1984) 2112.
[18] D. Kuhlmann, G. Masing, J. Raffelsieper, Z Metallkd. 40 (1949) 241.
[19] J. Friedel, Dislocations, Pergamon, Oxford, 1964.
[20] M. Verdier, Y. Bréchet, P. Guyot, Acta Mater. 47 (1999) 127.
[21] M. Hütter, G. Rutledge, R. Armstrong, Phys. Fluids 17 (2005) 014107.
[22] H. Zuidema, G. Peters, H. Meijer, Macromol. Theor. Simul. 10 (2001) 447.
[23] G. Eder, Nonlinear Anal., Theor. 30 (1997) 3807.
[24] G. Eder, H. Janeschitz-Kriegl, S. Liedauer, Prog. Polym. Sci. 15 (1990) 629.
[25] M. Hütter, Phys. Rev. E 64 (2001) 011209.
[26] M. Tobin, J. Polym. Sci. 12 (1974) 399.
[27] M. Tobin, J. Polym. Sci. 14 (1976) 2253.
[28] D. Turnbull, Trans. AIME 191 (1951) 661.
[29] B. Lustman, F. Kerze, The Metallurgy of Zirconium, McGraw-Hill, New York, 1955.
[30] C. Lemaignan, A. Motta, Zirconium alloys in nuclear applications, in: B. Frost (Ed.), Nuclear Materials, vol. 10b, VCH, 1994.
[31] R. Einziger, R. Kohli, Nucl. Tech. 67 (1984) 107.
[32] R. Einziger, S. Atkin, D. Stellrecht, V. Pasupathi, Nucl. Tech. 57 (1981) 65.
[33] P. Bouffioux, S. Leclercq, C. Cappelaere, T. Bredel, Interim dry storage of PWR spent fuel assemblies-development of a long term creep law to assess the fuel cladding integrity, in: International Conference on Radioactive Waste Management and Environmental Remediation. Bruges, 2001.
[34] C. Hunt, E. Schulson, J. Nucl. Mater. 92 (1980) 184.
[35] J. Derep, D. Rouby, G. Fantozzi, Revue de Métallurgie (11) (1981) 585.
[36] N. Rupa, Effet de l'hydrogene et des hydrures sur le comportement viscoplastique du Zircaloy-4 recristallisé, Université de Technologie de Compiègne, Compiègne, 2000.
[37] N. Dewobroto, N. Bozzolo, P. Barberis, F. Wagner, Mater. Sci. Forum., in: Conference Proceedings of Recrystallisation and Grain Growth Conference, Annecy, 2004, p. 453.
[38] D. Abson, J. Jonas, J. Nucl. Mater. 42 (1972) 73.
[39] J. Cahn, Acta Metall. 10 (1962) 789.
[40] M. Lee, J. Koo, Y. Jeong, Y. Jung, Korean J. Mater. Res. 9 (1999) 1123.
[41] M. Lee, Y. Jeong, Korean J. Mater. Res. 10 (2000) 725.
[42] H.S. Jeong, Y.M. Oh, Y.H. Jeong, S.J. Kim, Han'guk Chaelyo Hakhoechi 11 (2001) 104.
[43] K. Snowden, P. Stathers, D. Hughes, J. Nucl. Mater. 87 (1979) 297.
[44] J.C. Bokros, Germinative grain growth characteristics of zirconium, US Atomic Energy Comm., 1957, NAA-SR-1926.
[45] J. Herenguel, Le zirconium et ses alliages, Presses Universitaires de France, Saclay, 1962.
[46] C. Woods, R. Berman, F. Bingman, C. Busby, I. Cohen, R. Hoffman, S. Kass, O. Katz, J. Kearns, G. Salvaggio, E. Stofka, Properties of Zircaloy-4 tubing, Bettis Atomic Power Laboratory, Pittsburgh, 1966, Report: WAPD-TM-585.
[47] J. Derep, Etudes des proprietes mecaniques de 77 a 900 K et de la restauration–recristallisation de l'alliage Zircaloy-4. PhD thesis, Institut National des Science Appliquées de Lyon, 1981.
[48] L. Legras, Etude de la restauration/recristallisation du Zircaloy-4 au cours de recuits entre 400 °C et 520 °C. Formulation d'un premier modèle prenant en compte l'effet de l'hydrogene, EDF, Moret sur Loing, 1999.
[49] P. Merle, K. Loucif, L. Adami, R. Borrelly, J. Nucl. Mater. 208 (1994) 135.
[50] E. Steinberg, I. Pohlmeyer, A. Schaa, in: TopFuel '97 Conference Proceedings, vol. 2, Manchester, 1997, p. 65.
[51] M. Sauby, D. Lee, J. Nucl. Mater. 50 (1974) 175.
[52] S. Bush, R. Kemper, D. Gray, Recovery and recrystallization of zirconium and its alloys. Part 1 Specimen compositions, cold working, heat treatment and survey of the literature, Richland: Hanford Atomic Products Operation, 1961, Report: HW-69678.
[53] H. Rosinger, D. Northwood, J. Nucl. Mater. 79 (1979) 170.
[54] D. Northwood, I. London, L. Bahen, J. Nucl. Mater. 55 (1975) 299.
[55] N. Ashcroft, N. Mermin, Solid State Physics, Saunders College, Philadelphia, 1976.
[56] P. Soo, G. Higgens, Acta Metall. 16 (1968) 177.